Analysis of Counter-Rotating Wind Turbines

2007 J. Phys.: Conf. Ser. 75 012003

(http://iopscience.iop.org/1742-6596/75/1/012003)

Analysis of Counter-Rotating Wind Turbines

W Z Shen[1], V A K Zakkam[1], J N Sørensen[1] and K Appa[2]

[1] Department of Mechanical Engineering, Technical University of Denmark, 2800 Lyngby, Denmark

[2] Appa Renewable Energy Systems Incorporated, 22242 Anthony Drive, Lake Forest, CA 92630, USA

E-mail: shen@mek.dtu.dk

Abstract. This paper presents a study on the performance of a wind turbine with two counter-rotating (CRWT) rotors. The characteristics of the two counter-rotating rotors are on a 3-bladed Nordtank 500 kW rotor. The analysis has been carried out by using an Actuator Line technique implemented in the Navier-Stokes code EllipSys3D. The analysis shows that the Annual Energy Production can be increased to about 43.5 %, as compared to a wind turbine with a single rotor. In order to determine the optimal settings of the CRWT turbine, parameters such as distance between two rotors and rotational speed have been studied.

1. Introduction

When a traditional wind turbine with a single rotor system is used for energy conversion, only a part of the available energy in the wind is exploited. The maximum power that can be extracted from the wind is about 59% of the available energy, if the velocity change across the rotor, according to Betz theory [1], is 2/3. But in practice, the energy in the wake behind a single rotor is not very small. Part of this energy can be extracted further by installing a second rotor in the wake. At the same time, the maximum energy that can be extracted by two rotors of same diameters is increased from 59% to 64% of the available energy that is the Betz limit for two rotors. As the wake behind the first rotor is rotating in the opposite direction to the rotational direction of the rotor, the second rotor is advisable to rotate in the same direction as the wake in order to extract efficiently the available energy in the wake.

A contra-rotating wind turbine (CRWT) can be described as a system consisting of two rotors separated by an appropriate distance. One of the rotors is rotating in counter-clockwise direction and the other in clockwise direction. In 2002, Appa Technology Initiatives [2] has built a prototype in California and performed some field tests. The prototype model consisted of a 6 KW contra-rotating wind turbine system with two 2-bladed rotors. The results of these tests indicated that a contra-rotating turbine system could extract additional 30% power from the same wind stream. In 2005, Jung et al. [3] has considered experimentally and numerically (using the quasi-steady strip theory) a 30 kW CRWT that are consisted of an upwind auxiliary rotor of 5.5 m and a downwind main rotor of 11 m.

The current study involves numerical modelling and CFD computations of a counter rotating system. For general airflow past a wind turbine, it is straightforward to compute the solution by solving the steady/unsteady Navier-Stokes equations using RANS, DES or LES models on a structural mesh around the wind turbine of at least several million mesh points. These methods are very expensive and require a lot of computer memory. For a counter rotating wind turbine where two

rotors are rotating in opposite directions, the flow is usually unsteady. Moreover, the mesh needs to be split into two sub-meshes; each sub-mesh is confined with a rotor and between them a moving interface technique is required. Therefore, the computational cost will be much higher than that for a single rotor wind turbine. Due to our computer capacity, the actuator line model developed in [4] is chosen for the analysis. The actuator line model was developed for studying wind turbine power performance and wakes behind wind turbines. It combines a Navier-Stokes solver with a body force that is obtained from the blade element theory and tabulated airfoil data. Since the model does not need to solve the wall boundary layer of the wind turbine, an unstructured mesh of Cartesian or polar type is employed. In the current study, two 3-bladed rotors of equal diameters are used in the CRWT model.

2. Numerical method

The numerical model used for the analysis is called 'Actuator Line Technique'. The method combines an unsteady three-dimensional Navier-Stokes solver with a technique that considers each wind turbine blade by a body force that is distributed along a line from root to tip. The model has earlier been validated against measurements of a 500kW Nordtank wind turbine equipped with three LM19.1 blades [4].

2.1. Flow solver

The flow solver used here is the EllipSys3D code developed at the Technical University of Denmark (DTU) [5] in co-operation with the Department of Wind Energy at Risø National Laboratory [6]. The EllipSys3D code is based on a multi block / cell-centered finite volume discretization of the steady / unsteady incompressible Navier-Stokes equations in primitive variables (pressure-velocity). The finite volume method uses a predictor-corrector method. In the predictor step, the momentum equations are discretized using a second-order backward differentiation scheme in time and second-order central differences in space, except for the convective terms that are discretized by the QUICK upwind scheme. In the corrector step, a modified Rhie-Chow interpolation developed by Shen *et al.* [7] and a modified SIMPLE-C scheme on collocated grids [8] are used in order to avoid numerical oscillations from pressure decoupling. The obtained pressure Poisson equation is solved by a five-level multi-grid technique. For more details about the numerical technique, the reader is referred to the references [5]-[8]. The EllipSys3D code is based on a multi-block structure and is easily parallelized using Message Passing Interface (MPI).

For usual rotor computations, it is convenient to use cylindrical coordinates and to solve the flow equations in a frame attached to the rotor blades (moving frame). For computing flows past a CRWT where two rotors are rotating in the opposite directions, it is convenient to choose a frame fixed to one rotor and let the other rotor rotate in the frame. Thus, unsteady computations are unavoidable for this study. Since all variables are defined at cell centres, no special treatment is needed for the singularity problem at the centre axis. The boundary condition used at the outflow boundary is the convective boundary condition that consists of the convective part of the momentum equation.

2.2. Mesh

The computational domain is a polar grid with equal distance in azimuth direction, divided into a number of blocks with an equal number of mesh points in each direction. In the radial direction, the mesh is dense close to the blade tip and it increases exponentially towards the lateral boundary. In the axial direction, the mesh is dense close to the rotor plane with an exponential increase in mesh size towards the inflow and outflow planes. Since the rotor is 3-bladed, only one third of the azimuth domain is used, with periodic boundary conditions applied along the azimuth boundary.

The computational domain covers a domain $[0,8.5R]\times[0,2\pi/3]\times[-12.8R,13.8R]$ in radial, azimuth and axial directions, respectively where R is the rotor radius. The computational domain is divided into six blocks of 48x48x48, as shown in Fig. 1. The first rotor is placed at z=0 in the third block and the second rotor is placed some distance behind the first rotor in the wake.

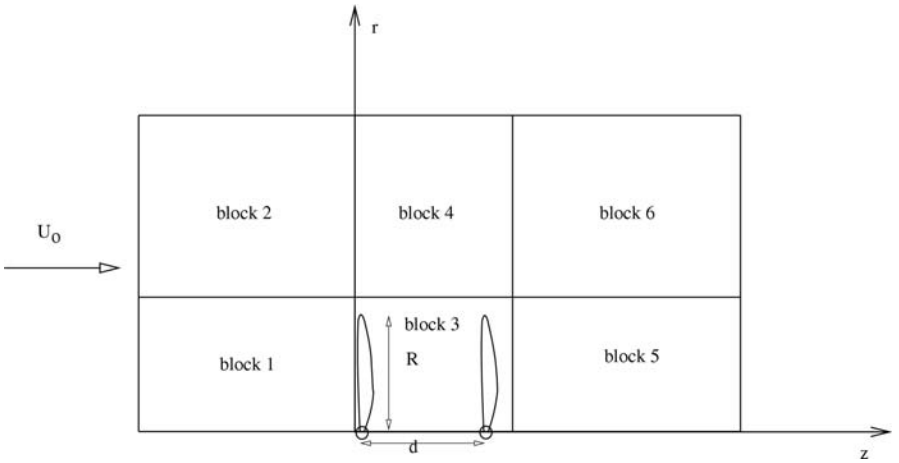

Figure 1: Block structure of the computational mesh at constant azimuth angle.

2.3. Actuator line technique

To determine the body forces on the rotor blades, we use a blade-element approach combined with two-dimensional airfoil characteristics. Since the first rotor is rotating with an angular velocity Ω_1, it is more convenient to let the system move with the same angular velocity. In the system (attached to the first rotor), the second rotor is rotating with an angular velocity of $\Omega_2 - \Omega_1$.

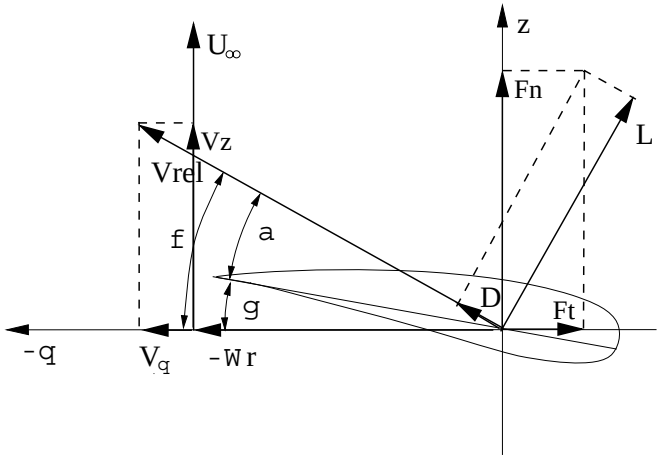

Figure 2: Cross-sectional airfoil element.

Denoting radial, azimuth and axial velocities in the rotating frame by V_r, V_θ and V_z, respectively, the flow angle on the first rotor is then determined (see Fig. 2) as

$$\phi_1 = \tan^{-1}\left(\frac{V_z}{-V_\theta}\right). \quad (1)$$

The angle of attack at each cross section is defined as $\alpha = \phi_1 - \gamma_1$ where γ_1 is the sum of local twist and pitch angles on the first rotor. The relative velocity is

$$V_{rel} = \sqrt{V_z^2 + V_\theta^2}\ . \quad (2)$$

The force per spanwise unit length is

$$\vec{f}_{2d} = \frac{d\vec{F}}{dr} = \frac{1}{2}\rho V_{rel}^2 c\left(C_l \vec{e}_L + C_d \vec{e}_D\right), \tag{3}$$

where $C_l = C_l(\alpha, \mathrm{Re})$ and $C_d = C_d(\alpha, \mathrm{Re})$ are the lift and drag coefficients, respectively. The lift and drag coefficients are determined from measured or computed two-dimensional airfoil data that are corrected for three-dimensional effects.

On the second rotor, the flow angle and the angle of attack are determined as

$$\phi_2 = \tan^{-1}\left(\frac{V_z}{(\Omega_2 - \Omega_1)r - V_\theta}\right) \tag{4}$$

$$\alpha = \phi_2 - \gamma_2$$

where γ_2 is the sum of local twist and pitch angles on the second rotor. The relative velocity is computed as

$$V_{rel} = \sqrt{V_z^2 + \left((\Omega_2 - \Omega_1)r - V_\theta\right)^2}\ . \tag{5}$$

The resulting force is distributed in the flow field by applying a regularization kernel, η_ε on

$$\vec{f}_\varepsilon(\vec{x}) = \sum_{n=1}^{3}\int_0^R \left[\vec{f}_{2d,rotor1}(r)\eta_\varepsilon\left(\vec{x} - \vec{x}_{rotor1,n}\right) + \vec{f}_{2d,rotor2}(r)\eta_\varepsilon\left(\vec{x} - \vec{x}_{rotor2,n}\right)\right]dr \tag{6}$$

where a regularization kernel is defined as

$$\eta_\varepsilon(r) = \frac{1}{\varepsilon^3 \pi^{3/2}}\exp\left(-\left(\frac{r}{\varepsilon}\right)^2\right). \tag{7}$$

2.4. Computational procedure

Computations are carried out in a procedure that combines the Navier-Stokes solver and the actuator line technique. It is summarized as

Step 1: Initialization: choose initial blade positions; initialize the velocity field with the free-stream velocity and the rotating speed; apply airfoil data to give initial blade forces using the initial velocity field.

Step 2: Solve the Navier-Stokes equations with a given volume force (EllipSys3D) at time *n*.

Step 3: Find the relative velocity and the angle of attack for rotor 1 and rotor 2 based on the velocity field from Step 2.

Step 4: Find the lift and drag coefficients for rotor 1 and rotor 2 by applying airfoil data at the actual angle of attack.

Step 5: Find the lift and drag forces from the relative velocity and the force coefficients in Step 4.

Step 6: Move the rotors to new positions.

Step 7: Find the volume force by using Eq. (6).

Step 8: Update the solution from time *n* to time *n+1* and go to Step 2.

3. Results and discussion

In order to analyze the performance of a CRWT turbine, our focus is mainly put on the turbine at a wind speed of 10 m/s, corresponding to a Tip-Speed-Ratio (TSR) of 5.81. The reason is that the reference turbine (Nordtank 500 kW) has a relatively high power coefficient at this wind speed. In the following sections, parametrical studies on distance between the two rotors (section 3.1) and rotational speeds of the CRWT system (section 3.2) are made at this wind speed. In section 3.3, computations at different wind speeds are carried out, followed by the Annual Energy Production (AEP) for the CRWT. The counter-rotating wind turbine (CRWT) is equipped with two Nordtank (500 kW) rotors. The first rotor is rotating anti-clockwise with an angular velocity of Ω_1 and the second rotor is rotating clockwise with an angular velocity of Ω_2. The diameter of the CRWT rotor is chosen to be 41 m,

corresponding to the diameter of a Nordtank 500 kW rotor. The distance between the two rotors can vary between 0 and 1 Radius of the rotor (R=20.5 m).

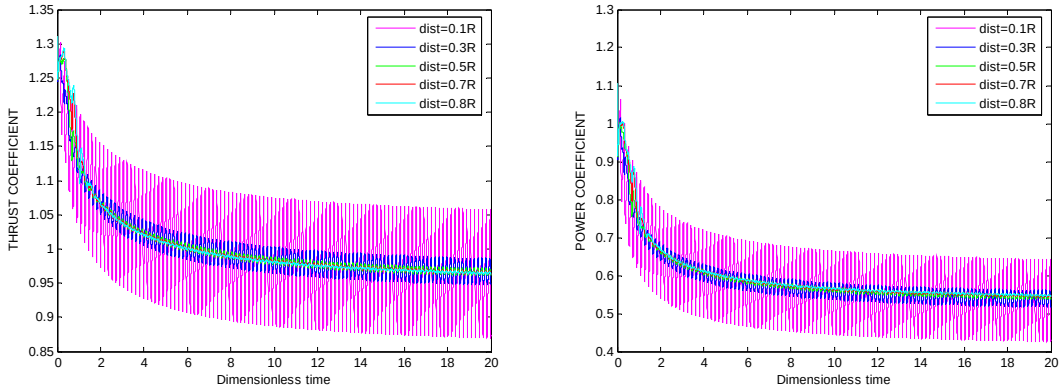

Figure 3: Thrust coefficient (left) and power coefficient (right) of the CRWT performed at wind speed of 10 m/s and various distances between two rotors.

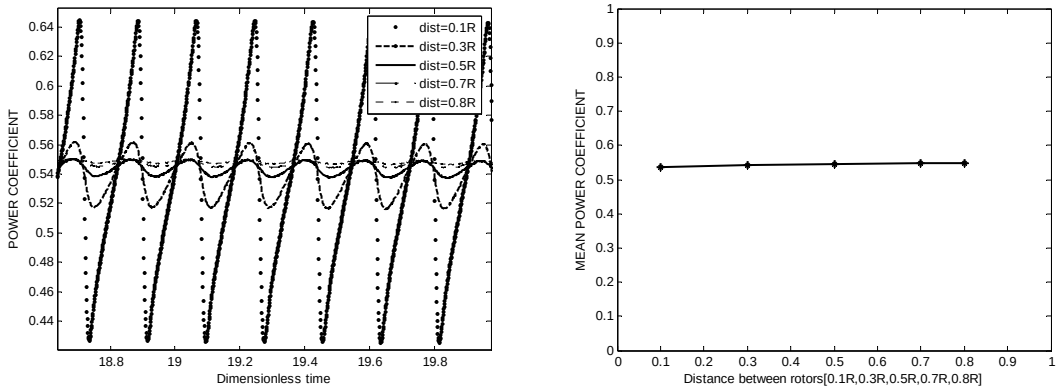

Figure 4: Zoomed power coefficient (left) and mean power coefficient (right) of CRWT at a wind speed of 10 m/s and various distances between the two rotors.

3.1. CRWT at various distances between two rotors

In this section, the distance between two rotors is analysed when they are exactly counter rotating ($\Omega_2 = -\Omega_1$). The thrust coefficient is plotted in Fig. 3 (left). From the figure, it is seen that the mean thrust coefficient ($C_T = \frac{2T}{\rho U_0^2 A}$) is independent of the distance between the two rotors, except that the thrust has a fluctuation when the distance is very close. The total power coefficient ($C_P = \frac{2P}{\rho U_0^3 A}$) of the CRWT is plotted in Fig. 3 (right). In contrast to the behaviour of the thrust coefficient, the power coefficient is seen to be slightly decreasing when the distance becomes small. At the distance of 0.1R, a large fluctuating power is seen. In order to see it clearly, the curves are zoomed and re-plotted in Fig. 4 (left). From the figure, all curves are seen to be fluctuating. The frequency of the oscillation is found to be the frequency of blade passing between the two rotors ($f = (\Omega_1 - \Omega_2)N/2\pi = 5.55$ where N is the number of blades or a time period of T=0.18). The

mean power coefficient is plotted in Fig. 4 (right). From the figure, it is seen that Cp is almost independent of the distance.

3.2. CRWT at various rotational speeds (Ω_1=-Ω_2=27.1, 19.5, 14.6, 9.8, 4.9 rpm)

In this section, the rotational speed of the CRWT is varying while the wind speed is kept constant at 10 m/s. The distance between two rotors is 0.5R. In this study, only the exact counter rotation is considered. The rotational speeds are 27.1, 19.5, 14.6, 9.8 and 4.9 rpm. In Fig. 5 (left), the power coefficient is plotted. From the figure, it is seen that the total power coefficient is decreasing significantly when the rotational speed decreases. Same feature can be observed in the thrust coefficient (Fig. 5 (right)). It is also seen that the thrust has a fluctuation at very low tip speeds.

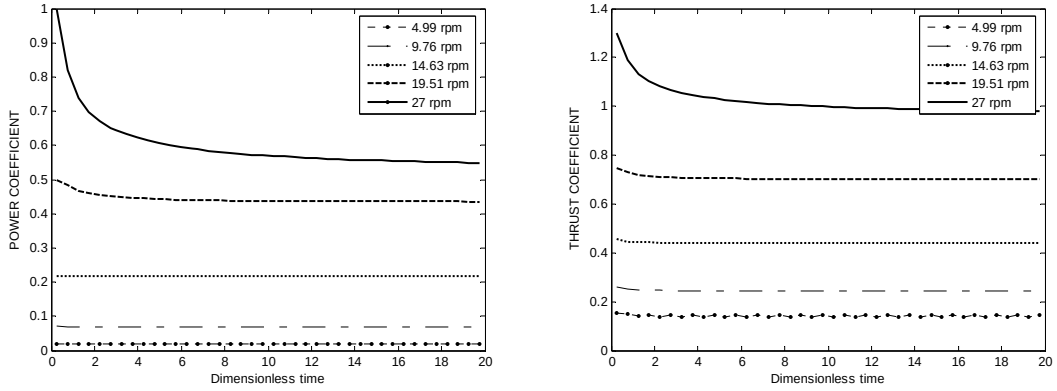

Figure 5: Power coefficient (left) and thrust coefficient (right) of the CRWT performed at wind speed of 10 m/s and various rotational speeds.

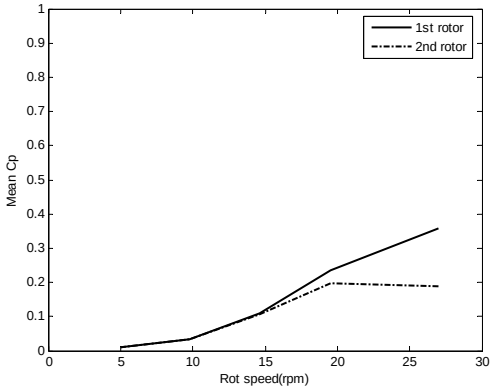

Figure 6: Mean power coefficient of the CRWT performed at wind speed of 10 m/s and various rotational speeds.

The mean power coefficients of the individual rotors are plotted in Fig. 6. From the figure, it can be seen that the power coefficient of the second rotor is smaller than that of the first one at high rotational speeds. When the rotational speed decreases to 19.5 rpm, both rotors have almost the same power coefficient. The interesting thing is that the total power coefficient of the CRWT is almost double as high as for a single rotor.

3.3. Annual Energy Production of a CRWT

In order to estimate the Annual Energy Production (AEP) of a counter rotating wind turbine, wind speed data, measured from a 70 m mast on the island of Sprogø in Denmark, are used. The data are averaged in a time interval of 10 minutes. The wind speed distribution in the range 0 to 25 m/s is plotted in Fig. 7. From the figure, it is seen that the distribution can be approximated by the Weibull distribution:

$$f(x) = \frac{s}{a}\left(\frac{x}{a}\right)^{s-1} \exp\left[-\left(\frac{x}{a}\right)^{s}\right]$$

where x is wind speed, s is the shape parameter (or slope) and a is the scale parameter. For the distribution in Fig. 7, the Weibull parameters can be fitted as: a=9.3966 and s=2.1879.

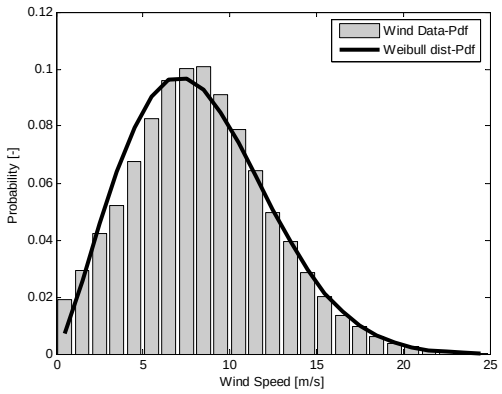

Figure 7: Wind speed distribution measured in the island of Sprogø [9].

The mean power coefficient is obtained from the computations performed using EllipSys3D code. From the power coefficient, the power outputs of a CRWT and a single rotor wind turbine (SRWT) with a radius of 20.5 m are calculated and plotted in Fig. 8.

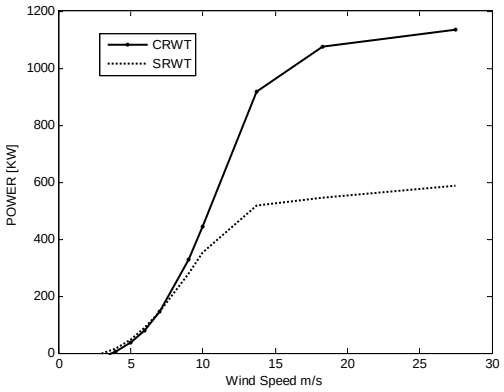

Figure 8: Power curves of CRWT and SRWT with a radius of 20.5 m.

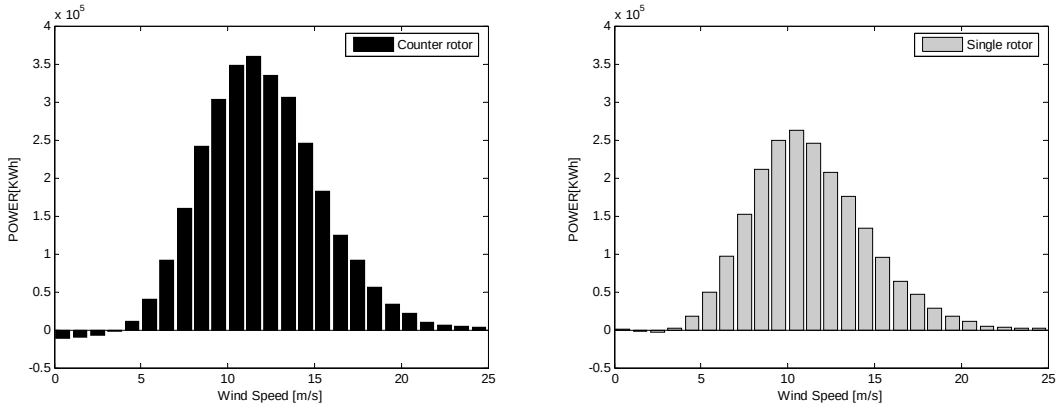

Figure 9: Discrete annual energy production of CRWT and SRWT located in the island of Sprogø, Denmark.

Using the wind speed distribution in Fig. 7, the annual energy production is calculated and plotted in Fig. 9. From the figures, it is seen that the CRWT produces more energy in most of the wind speed range. Making integration from 5 m/s, it is found that the AEP of the CRWT is 2965.9 MWh, whereas the AEP of the SRWT amounts to 2066 MWh. The increase of AEP is 43.5%.

4. Conclusion

The performance of a CRWT equipped with two Nordtank 500 kW turbines is studied. The main result of the study is that CRWT performs quite well at high wind speeds. At low wind speeds, it is suggested to reduce the rotational speed of the CRWT in order to capture more energy. For a counter rotating wind turbine operated on the island of Sprogø, Denmark, it can produce 43.5 % more annual energy than a single rotor turbine of same type. The performance of the CRWT can be improved if it is operated for low wind speeds at the tip-speed-ratio where a maximum Cp is obtained.

Since a modern wind turbine has a high power coefficient (> 0.5), it would be interesting to consider the efficiency of a CRWT equipped with two modern wind turbine rotors. From current knowledge, it can be estimated that at wind speeds where a maximum Cp is obtained, the power increase of using a CRWT instead of a SRWT may be a bit smaller, but at high wind speeds, it would work alike the present case. The overall annual energy production of the new CRWT system would increase less importantly.

Acknowledgement

The study of the contra rotor wind turbine system was funded by the Appa Renewable Energy Systems Incorporated, California, USA.

References

[1] Betz A 1920 *Zeittschrift für das gesamte turbinewessen* 307-309.
[2] Appa K 2002 *Energy Innovations Small Grant (EISG) Program (Counter rotating wind turbine system)* Technical Report, California, US.
[3] Jung S N, No T S and Ryu K W 2005 Renewable Energy **30** 631.
[4] Sørensen J N and Shen W Z 2002 *Journal of Fluids Engineering,* **124** (2) 393.
[5] Michelsen J A 1992 *Basis3D - a Platform for Development of Multiblock PDE Solvers* Technical Report, AFM 92-05, Technical University of Denmark, Denmark.
[6] Sørensen N N 1995 *General Purpose Flow Solver Applied to Flow over Hills* Risø-R-827-(EN), Risø National Laboratory, Roskilde, Denmark.
[7] Shen W Z, Michelsen J A and Sørensen J N 2001 *AIAA Journal* **39** 2406.
[8] Shen W Z, Michelsen J A, Sørensen N N and Sørensen J N 2003 *Numerical Heat Transfer* B **43** 221.
[9] http://www.winddata.com, a database on wind characteristics.